# Nano-coating protects biofunctional materials

The demand to develop convergent technology platforms, such as bio-functionalized medical devices, is rapidly increasing. However, the loss of biological function of the effector molecules during sterilization represents a significant and general problem. Therefore, we have developed and characterized a nano-coating (NC) formulation capable of maintaining the functionality of proteins on biological-device combination products. As a proof of concept, the NC preserved the structural and functional integrity of an otherwise highly fragile antibody immobilized on polyurethane during deleterious sterilizing irradiation ($\geq$ 25 kGy). The NC procedure enables straight-forward terminal sterilization of bio-functionalized materials while preserving optimal conditioning of the bioactive surface.

Rupert Tscheliessnig[1,2], Martin Zörnig[3], Eva M. Herzig[4], Katharina Lückerath[3], Jens Altrichter[5], Kristina Kemter[5], Adnana Paunel-Görgülü[6], Tim Lögters[6], Joachim Windolf[6], Silvia Pabisch[7], Jindrich Cinatl[8], Holger F. Rabenau[8], Alois Jungbauer[1], Peter Müller-Buschbaum[4], Martin Scholz[5,6]* and Joachim Koch[3]*

[1]University of Natural Resources and Applied Life Sciences, Vienna, Austria; [2]Austrian Centre of Industrial Biotechnology, Vienna, Austria; [3]Georg-Speyer-Haus, Institute for Biomedical Research, Frankfurt am Main, Germany; [4]Lehrstuhl für Funktionelle Materialien, Technische Univerität München, Garching, Germany; [5]Leukocare AG, München, Martinsried, Germany; [6]Department of Traumatology and Hand Surgery, Heinrich-Heine University, Düsseldorf, Germany; [7]Faculty of Physics, University of Vienna, Austria; [8]Institute for Medical Virology, Johann Wolfgang Goethe-University, Frankfurt am Main, Germany
*E-mail: joachim.koch@em.uni-frankfurt.de, martin.scholz@leukocare.com

The most common sterilization procedures for bio-functionalized medical devices (e.g., implants) for clinical use[1-3] are β-irradiation (electron beam), γ-irradiation, and ethylene oxide (EtO) gas sterilization. However, these procedures might lead to high energy transfer and altered protein folding attributable to loading shifts, redistribution of charges within the protein, loss of hydrogen bonds, and cleavage of covalent bonds within the protein[4-8]. Especially with β- and γ-irradiation, the presence of oxygen and water facilitates the formation of destructive oxygen radicals[7,9] and the high energy transfer may lead to unfolding and aggregation of the protein.

Therefore, new approaches to avoid sterilization-mediated damage of bio-functionalized materials are urgently needed. We have developed a nano-coating (NC) procedure for the stabilization and protection of biofunctionalized materials. NC is devoid of sugars, sugar alcohols, and proteins which are commonly used as an excipient in pharmaceutical liquids and freeze-dried formulations[10-13], but do not inhibit sterilization-mediated protein denaturation. By contrast, the NC solution comprises biocompatible small molecules and glycyrrhicic acid that form a protecting layer on the surface of the biofunctionalized material after drying.
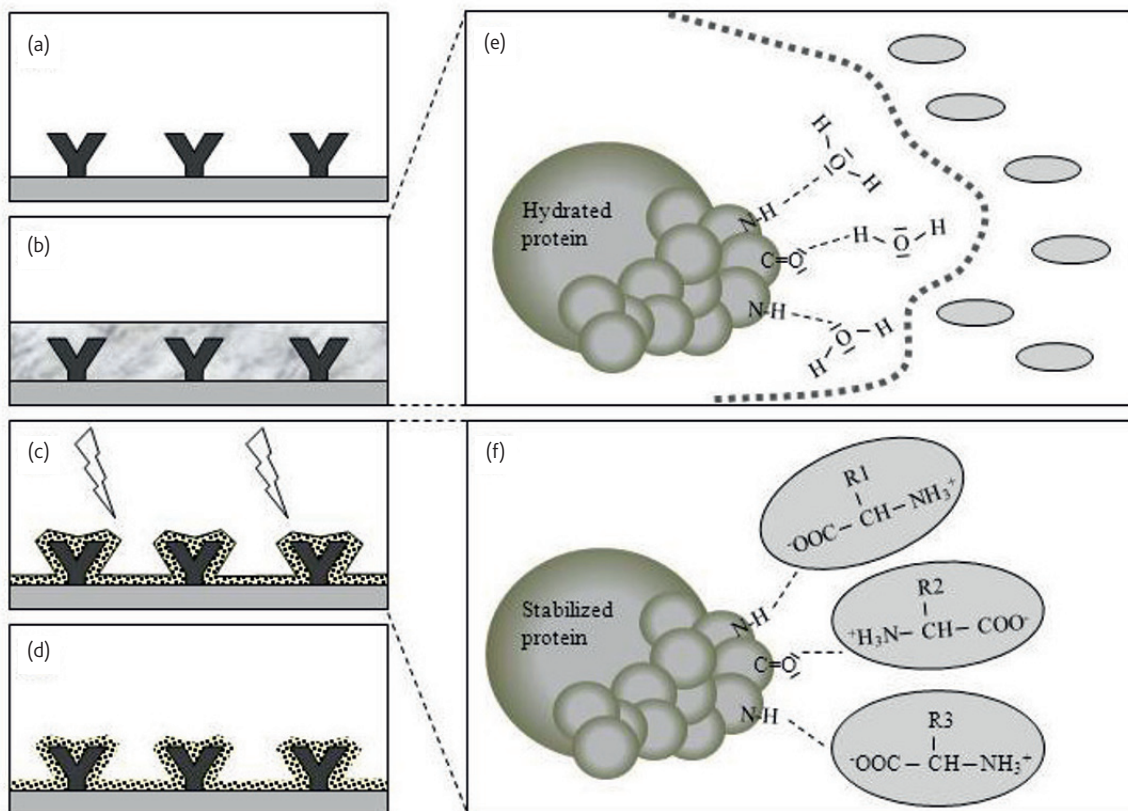
*Fig. 1 Fabrication process of a bio-functionalized surface and its protection from radiation-mediated damage. The chemical interactions between protein, water, and co-solutes are depicted schematically. Co-solvents provide hydrogen bonds and substitute for water molecules. (a) Surface with immobilized protein, (b) incubation with stabilizing co-solvent, (c) irradiation of dried surface, (d) rehydration, removal of co-solvent, (e) preferential hydration of protein and exclusion of co-solvent (grey ovals), (f) stabilization of protein by hydrogen bonding to co-solvent molecules.*

The protecting efficacy of the NC procedure is assumed to be in accordance with the concepts of preferential exclusion and preferential binding[10,14-18] as depicted in Fig.1. Biomolecules, immobilized on a biocompatible carrier (Fig. 1a) are embedded in the NC solution (Fig. 1b). After drying, the biofunctionalized material can be stressed, e.g., by irradiation (Fig. 1c) without loss of molecular integrity (Fig. 1d). It is therefore appreciated that the stabilizing excipients support a preferentially hydrated, native protein conformation in the liquid phase (Fig. 1e). Upon drying of the bioactive surface, excipients should substitute for water molecules at the protein surface by forming hydrogen bonds between the protein and the functional groups of the co-solvent (Fig. 1f). A glassy molecular film of co-solvent established at the end of the drying process, is considered to protect the functionality of the surface.

As proof of concept, the multimeric and fragile anti-Fas IgM antibody (IgM$_{Fas}$, 900 kD) was covalently coupled to open porous polyurethane (PU) for the use in a medical device for extracorporeal immunotherapy. The antibodies used here agonistically recognize and stimulate Fas (CD95)[19] on circulating hyper-activated neutrophils (most abundant white blood cells

in humans) from severely ill patients to limit systemic inflammation[19-21].

In order to protect radiation-sensitive PU-IgM$_{Fas}$ during sterilization of the support, we tested the nano-coating formulation and determined i.) physico-chemical characteristics ii.) molecular mechanisms of protein stabilization, and iii.) safety and efficacy.

This nano-coating formulation can now be applied for the production of improved bio-functionalized medical devices and will ease the application of biomedical combination products.

## Experimental
### Materials and methods
#### Nano-coating solution
The nano-coating solution (Leukocare, Munich, Germany) was fabricated by specifically combining different non-toxic small molecules (here, amino acids) and glycosidic excipients (here, glycyrrhizic acid) to reach a stock concentration of 100 g/L (pH 7.2) and a final solution of 25 g/L.

#### *Fabrication of bio-functionalized PU surfaces*
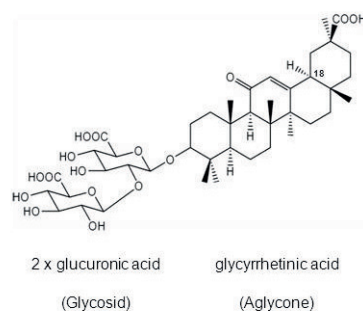Open porous medical-grade polyurethane foams (KCI, San Antonio, TX,

*Fig. 2 Formula of glycyrrhizic acid. (3β,18α)-30-hydroxy-11,30-dioxoolean-12-en-3-yl 2-O-β-D-glucopyranuronosyl-β-D-glucopyranosiduronic acid.*

USA) were cut into 3 cm$^3$ cylindrical samples and incubated with 2 % glycidoxypropyl-trimethoxysilane (Sigma, Deisenhofen, Germany) in methanol for 90 min. After air drying and coupling of anti-Fas IgM (4 μg/mL, clone CH11,) nano-coating was performed by 30 min incubation and subsequent drying (90 min). Sterilization was performed with β-irradiation at 25 kGy (BGS, Bruchsal, Germany).

**X-ray diffraction**
An x-ray diffractometer XRD 3000 TT (Seifert, Germany) equipped with a copper anode (40 kV, 30 mA, wavelength 0.154 nm) and a scintillation counter was used. The dried films or lyophilized (about 30 mg; powder diffraction) products were placed in the sample carrier and analyzed in the angular range from 5º to 45° 2θ, with steps of 0.05° 2θ and duration of 2 s per step. The analyses were performed by Coriolis Pharma Service GmbH (Munich, Germany).

**Differential scanning calorimetry**
Differential scanning calorimetry (DSC) in a Mettler Toledo 821e (Giessen, Germany) was used to determine the glass transition temperature of the maximally freeze-concentrated solution ($T_g'$) of the liquid formulations and the glass transition temperature $T_g$ of the lyophilized cakes. The $T_g'$ samples were cooled to –80 °C at a cooling rate of approximately 10 K/min. The midpoint of the endothermic shift of the baseline was taken as $T_g'$ (Coriolis Pharma Service). To determine the $T_g$, 10 mg of the freeze-dried cake was analyzed in crimped Al-crucibles. The samples were cooled to 0 °C with 10 K/min and reheated to 120 °C with a scanning rate of 10 K/min. The midpoint of the endothermic shift of the baseline during the heating scan was taken as $T_g$.

**Spectral reflectance**
Thin film characteristics were measured by reflecting light off the film and analyzing the resulting reflectance spectrum over a range of wavelengths (Filmetrics Inc., Munich, Germany).

**Viscosity measurements**
The viscosity of the samples was determined using a falling ball viscometer (model AMVn, Anton Paar, Ostfildern, Germany) at 25 °C an angle of α = 60° (Coriolis Pharma Service).

**Film thickness measurements**
To determine the thickness of the samples on PU-covered substrates x-ray reflectivity (XRR) was carried out with a Bruker D8 reflectometer. The measurements were carried out using monochromatic x-rays with a wavelength of 0.154 nm (Cu-Kα radiation) in a θ/2θ setup with optimized slit settings for high resolution. The thicker films were characterized using a profilometer (Veeco, Dektak 3030).

**Small-angle x-ray scattering (SAXS)**
SAXS experiments were performed with Cu-Kα radiation emitted by a rotating anode generator (Nanostar, BRUKER AXS). The system was equipped with a pinhole camera and an area detector (VANTEC 2000). Samples were fixed onto a stage-holder. The SAXS intensity patterns were taken at a sample-to-detector distance of 109 cm for 20 min to 6 h. All data were corrected for background scattering and then radially averaged to obtain the function I(Q), where Q = (4π/λ)sinθ is the scattering vector, 2θ is the angle between the incident and diffracted beam, and l = 0.1542 nm is the x-ray wavelength. We chose the homologous solution structure of human IgM (2RCJ)[22] as the initial configuration, to which SAXS fit and applied an in-house fitting code[23,24]. Using an MC algorithm, we randomly created scatters with the restriction that their position was within a size limit of 2 nm with respect to the homologous model. The homologous model was thus refined by the SAXS data but served as a permanent corrective of the numerical reconstruction procedure after each step. The final fitted scattering curves for the monomer and the self-assemblies are provided.

**Sterilization**
Sterilization was performed by Beta-Gamma Service (Bruchsal, Germany) using β-irradiation at 25 – 40 kGy. Sampling was performed by sterile rinsing of the housings and collecting the fluids in a sterile container. After membrane filtration of the samples, membranes were transferred to CASO Agar plates for the determination of colony-forming units of aerobic bacteria, fungi, and spore-forming bacteria. The analysis was performed by Medical Device Services (MDS, Munich, Germany).

**Virus infectivity assay**
For the infectivity/inactivation study, adenovirus type 5[25-27], strain Adenoid
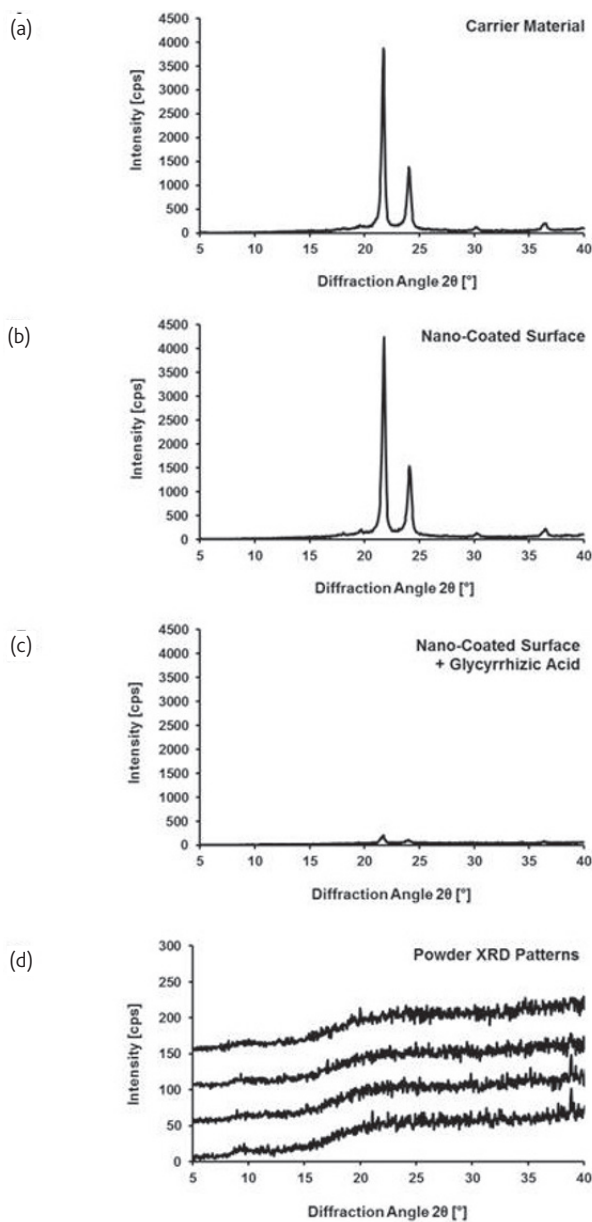
(a)



(b)



(c)



(d)



*Fig. 3 Wide-angle x-ray diffraction patterns and wide-angle x-ray powder diffraction patterns. (a) X-ray diffraction patterns of a non-coated surface with four characteristic peaks for the used carrier material. (b) A nano-coated surface without glycyrrhizic acid (amorphous structure). (c) A nano-coated surface with glycyrrhizic acid (amorphous structure; coating covers diffraction signal of the non-coated carrier), and (d) X-ray powder diffraction patterns of freeze-dried antibody samples in the presence of nano-coating.*

75 (American Type culture collection, ATCC-VR-5) was propagated on the human lung cancer cell line A549 (ATTC-CCL-185) in minimum essential medium (MEM) with 5 % fetal calf serum (FCS). The virus titer was determined by means of end-point titration (eight wells per dilution in a
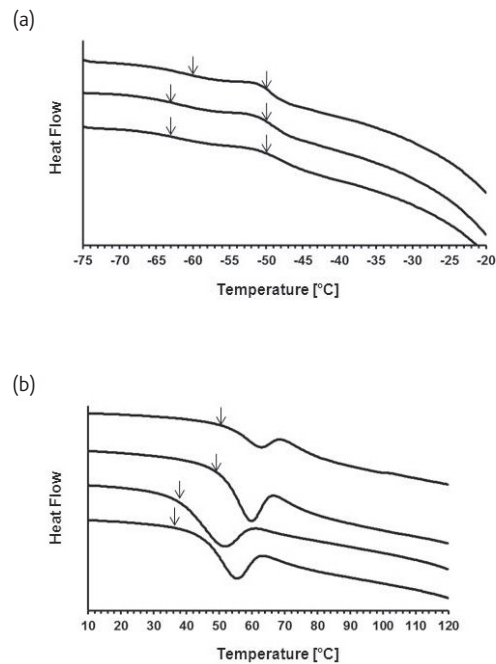
(a)



(b)



*Fig. 4 Thermograms of differential scanning calorimetry (DSC). (A) Frozen nano-coating (NC) without glycyrrhizic acid (GA; top), with GA (2 mg/ml, middle; 5 mg/ml, bottom) showing two glass transition points (arrows). GA decreases the lower $T_g'$. (B) DSC of freeze-dried antibodies in the presence of NC with and without $\beta$-irradiation. NC was mixed with different antibody amounts (ratio of 1.2:1) prior to freeze-drying; untreated (first and third curve from top) or $\beta$-irradiated (first and third curve from bottom) before DSC.*

96-well microtiter plate), with 50 mL virus dilution and 50 $\mu$L A549 cells (1-1,5 x $10^4$ cells) per well. A titer of 1,1 x $10^9$ tissue culture infectious dose (TCID50)/mL was used. Specifically, a volume of 50 mL virus suspension was dried at 37 °C on the bottom of sterile polystyrol tubes. The dried virus was then overlaid by 50 mL of the protective solution and dried again at 37 °C. After $\beta$-irradiation at 25 kGy or 40 kGy (controls were not irradiated), the virus/protective solution bilayer was resuspended in 1 mL MEM. The virus titer was determined again as described above. Cytopathic effects (CPE) were quantified after 7 days. Virus controls were treated identically but without $\beta$-irradiation.

### Functional characterization

For the quantification of immobilized IgM, an enzyme-linked immunosorbent assay (ELISA) was developed. For detection, a horseradish peroxidase (HRP)-conjugated goat-anti-mouse IgM antibody was used. TMB (3,3',5,5'-tetramethylbenzidine; Sigma) was used for substrate reaction.

Recombinant hFas:Fc protein was purified from stably transfected Chinese hamster ovary cells (expression plasmid ps299-hFasFc kindly provided by Pascal Schneider, Lausanne, Switzerland)28 using HiTrap Protein A column one-step purification according to standard procedures. The bioactivity of hFas:Fc was tested by inhibiting FasL-mediated cell death of RKO cells (human colon carcinoma cell line) and flow cytometric
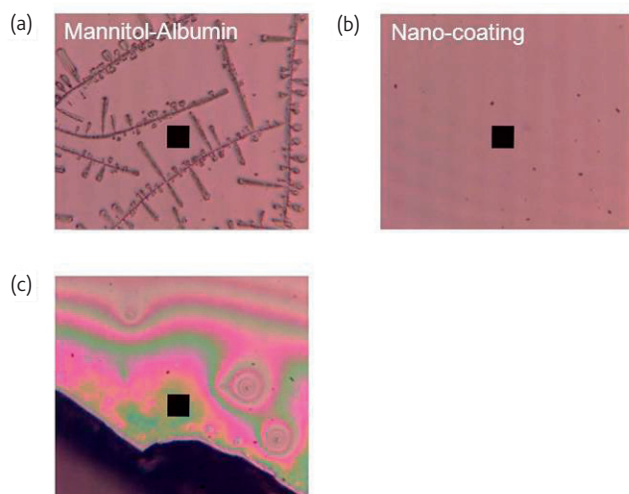
Fig. 5 Spectral reflectance analyses of nano-coating on Si. (a) Photomicrographs of a dried mannitol-albumin mixture (crystalline) and (b) nano-coating (amorphous) on Si.
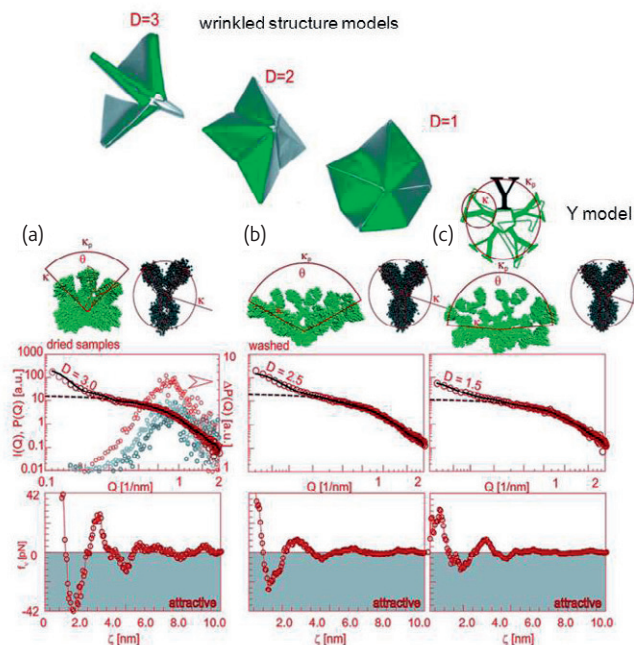


Fig. 6 SAXS images of functionalized open porous polyurethane foam. The fractal dimensions of the IgM are depicted by the wrinkled structure models (top) and the self-similarity (Y shape of IgG arms) by the Y model. Reconstructed IgG (gray bead model) and IgM (green bead model) are shown. The medium panel (large red open circles) shows background-corrected scattering intensities. Dashed lines indicate analytic form factors. Black lines give the full fit of SAXS data based on the gray IgG structural models and their mean forces. In the lower panel, small open connected circles indicate corresponding mean forces. (a) Dried *PU-IgM$_{Fas}$, PU-IgM$_{Fas}$–NC, and *PU-IgM$_{Fas}$–NC samples (*β-irradiation). The relative change of their form factors ΔP(Q) with respect to PU-IgM$_{Fas}$ are given (small red, gray, and black open circles, respectively). For D = 3, the mean forces hold a pronounced corrugation and are given as a multitude of kT, where k is the Boltzmann constant and T is the system temperature. (b) The sample PU-IgM$_{Fas}$ was rehydrated (D = 2.5) and the corrugation of the corresponding mean force decreased. (c) The rehydrated samples of *PU-IgM$_{Fas}$ could not be analyzed (no signal) whereas *PU-IgM$_{Fas}$–NC samples exhibited a fractal dimension of 1.5 and a decreased corrugation of the corresponding mean force.

quantification of cells with hypoploid DNA content by propidium iodide staining[29].

Peptide arrays of isoform 1 of human Fas (aa 1-177 and permutated peptides; accession no. P25445) were synthesized by Fmoc chemistry at activated PEG-spacers on cellulose membranes by automated parallel peptide synthesis on a MultiPep RS instrument (Intavis, Köln, Germany) as described previously[30-34]. Interaction studies with antibodies were performed according to published procedures[33,35]. Bound antibodies were visualized by chemiluminescence imaging. Selected soluble epitope peptides carrying N-terminal biotinylation were obtained from Diana Imhof (Institute of Biochemistry, University of Jena, Germany).

For affinity measurements, IgM$_{Fas}$ was immobilized on an ELISA plate (with and without β-irradiation and/or nano-coating) and probed with graded amounts of epitope peptide (biotin-RCKPNFFCNSTVCEHCDP-NH2), which was subsequently detected by a streptavidin-HRP conjugate in a colorimetric assay. For K$_D$ determination, data were fitted to a 1:1 Langmuir binding model.

Fas-negative and Fas-positive T-cells (Jurkat cell line) and freshly isolated neutrophils from trauma patients (study approval was obtained from the Ethics Review Board of the University of Duesseldorf, Germany) were challenged with PU-IgM$_{Fas}$ for 4 h. Subsequently, cells were harvested, and the number of cells which had undergone programmed cell death (apoptosis) was determined by staining the cells with propidium iodide and flow cytometric analysis[29].

**Statistics**

All experiments were done at least five times. Where relevant, data are presented as mean +/- SDM. Statistical analyses were performed by Student's t-Test (GraphPad Prism Program, version 5, GraphPad Software, San Diego, CA). P values of less than 0.05 were considered statistically significant.

## Results
### Biofunctionalization of PU with IgM and nano-coating
The biofunctionalization of the PU surface comprised three major steps. In step 1, PU was treated with the commonly used glycidoxypropyl-trimethoxysilane to enable the covalent binding of the IgM antibody to the surface (step 2). After covalent coupling of the antibody to the surface the nano-coating solution is added to cover the PU surface and the antibody (step 3). During drying of the coated surface (PU-IgM$_{Fas}$-NC) the excipients in the nano-coating solution substitute the water molecules around the IgM and by this form a protecting shell to stabilize the protein under stress conditions. These procedures and the stabilizing mechanisms of the nano-coating are schematically depicted in Fig. 1. The procedures to covalently couple biomolecules and the concept of nano-coating can

| Application | Biomaterial (carrier) | Biomolecule |
|---|---|---|
| Orthopedic and dental implants | Titanium | Bone morphogeneic protein-2<br>Antimicrobial proteins |
| Cardiovascular stents | Steel | IgG antibodies |
| Wound dressings | Polyurethane<br>Polyester<br>Polyvinyl alcohol (PVA) | Proangiogenic growth factors<br>Ascorbic acid |
| Catheters | Steel<br>Gold<br>Gold/Hydrogel combination<br>Titanium alloys | IgG antibodies<br>Antibody fragments |
| Extracorporeal blood treatment devices and circuit components | Polyurethane<br>Polyester<br>Polycarbonate | Anti-Fas IgM |
| Bio-functionalized micro- and nano-beads | Polyethylene<br>Glass<br>Silicium | IgG antibodies |
| Diagnostic devices | Silicium | IgG antibodies<br>Circulating free DNA |
| Protein arrays | Polycarbonate<br>Polystyrol<br>Polytetrafluorethene<br>Glass | Proteins range: 9-900 kDa |
| Formulation of therapeutic antibodies and biopharmaceuticals | Lyophilisates | IgG and IgM antibodies |
| Vaccine generation and formulation | Lyophilisates | Viruses and viral antigens |

be applied to a broad range of biocompatible materials as listed in Table 1. The following chapters focus on the physical characterization and the functionality of the nano-coating and the embedded IgM antibody.

**Physical characteristics of the nano-coating formulation**
The physical nature (crystalline or amorphous characteristics) of the newly developed nano-coating formulation was examined using wide-angle x-ray diffraction of dried nano-coating films on a carrier material and wide-angle powder x-ray diffraction of freeze dried antibody/nano-coating mixtures. XRD is a commonly used method to characterize the physical morphology of dried films or powders, respectively. The differential scanning calorimetry (DSC) of the maximal freeze concentrated solutions and of the freeze-dried powders is a complementary method. Spectral reflectance, x-ray reflectivity (XRR), and profilometer were used to determine homogenicity and thickness of the dry film (nano-coating).

The XRD patterns (Fig. 3) of the non-coated surfaces showed two main characteristic peaks and three smaller peaks for the used carrier material (Fig. 3a). Nano-coating of this material with co-solvent solution devoid of GA resulted in the same XRD pattern, suggesting an amorphous structure without additional crystallization peaks (Fig. 3b). The decrease of intensity of these characteristic peaks in the XRD pattern by supplementation of the nano-coating solution with GA may be associated with a more pronounced amorphous character and could provide evidence for a higher coating thickness (Fig. 3c). In addition, the physical property of the nano-coating solution in combination with antibodies in the dried state was analyzed by wide-angle x-ray powder diffraction. The antibody solids, freeze-dried in the presence of nano-

coating solution, displayed halo powder XRD patterns (Fig. 3d), which are typical for non-crystalline solids. The absence of peaks suggests that the analyzed samples were present in an amorphous state.

The study of the thermal behavior during freezing and in the dried state by Differential Scanning Calorimetry (DSC) was a complementary approach to the examination of the physical property of the nano-coating formulation. Determination of a glass transition temperature of the maximally freeze-concentrated phase $T_g$' and a glass transition temperature of the corresponding solid $T_g$ without any additional characteristic crystallization event in the monitored thermograms further indicate the amorphous character of the nano-coating formulation during freezing and in the dried state.

Analysis of the frozen co-solvent solution by differential scanning calorimetry (DSC) revealed two thermal transitions of the freeze-concentrated non-ice phase ($T_{g1}$' at −49 °C and $T_{g2}$' at −60 °C), which are typical for amino acids. No characteristic crystallization events were found in the thermograms of the frozen nano-coating (Fig. 4a) indicating a formation of an amorphous phase upon freezing. Only a minor decrease of $T_{g2}$' due to the addition of increasing amounts of GA without any influence on the amorphous state was observed. Additionally, the DSC thermograms of antibody solids, freeze-dried in the presence of nano-coating, were consistent with amorphous solids without any evidence of crystallization (Fig. 4b). The observed shifts of the glass transition temperatures $T_g$ are a consequence of different amounts of solid during lyophilization, associated with a different residual moisture content with a high impact on stability, shelf life and favorable storage temperature (data not shown).

To define thin film characteristics of different coatings (Fig. 5)

spectral reflectance of coated silicon showed crystallization of mannitol in a mannitol-albumin mixture (Fig. 5a), whereas a homogenous film was formed in the presence of nano-coating (Fig. 5b).

NC films on silicon and PU were analyzed by falling ball viscometry and displayed a viscosity of 1.15 mPa·s which is similar to water (0.89 mPa·s). This viscosity allows easy handling and homogenous distribution of the nano-coating formulation during the coating procedure of solid materials and of embedded biomolecules. Silanisation and the coupling of the anti-Fas IgM resulted as expected in very thin layers, resolvable in XRR. However, for the thicker nano-coating the Kissing fringes vanished due to the interplay of increased thickness and sample roughness. Therefore the nano-coating thickness of the various films was additionally probed with a profilometer (Veeco, Dektak 3030). The combination of both methods, XRR and profilometer measurements, allowed a reliable determination of the relevant film thicknesses. The anti-Fas IgM coupled on the PU with a film thickness of 60 nm and the nano-coating itself formed thicker films in the range of 250 – 350 nm in this planar geometry.

**Structural stabilization of immobilized anti-Fas IgM by nano-coating as monitored by small-angle x-ray scattering (SAXS)**

SAXS is a diffraction method that permits the study of the overall structure of randomly oriented macromolecules. The radial average of the detected scattering profile results in the scattering curve $I(Q)$, measured in reciprocal space of nm$^{-1}$, where $Q = (4\pi/\lambda)\sin\theta$ is the scattering vector, $2\theta$ is the angle between the incident and diffracted beams, and $\lambda$ is the x-ray wavelength. These parameters give the molecular mass of a protein, the size of a protein ($R_G$; radius of gyration), the maximum dimension of the hydrated macromolecule, and its shape in real space ($P(r)$; distance distribution function). Constraint modeling enables the direct calculation of structural models, from the known atomic structure (e.g., from crystallography) and the fitting of the experimental scattering curves.

In this study, the new concept of constraint modeling based on the theory of self-similarity and fractal mean force potential for the reconstruction of the immobilized IgM structures[23,24] was applied. Using this model, the IgM pentamer is mathematically considered self-similar and thus corresponds to a fractal scattering profile. The self-similarity of the IgM molecule at different length scales is based on its characteristic Y-like structure (Fig. 6, Y model).

The three-dimensional structure of the anti-Fas IgM molecule covalently coupled to open porous polyurethane (PU) foam after drying, $\beta$-irradiation, and rehydration (Fig. 6) was analyzed by SAXS[23,24]. Background-corrected scattering contrasts, $I(Q)$, of the dried and rehydrated samples (Fig 6a-c, medium panel, large red open circles) were obtained by determination of the PU background alone. The fit of these experimental data, gives the shape of the coupled IgM molecule in the real space, the form factor ($P(Q)$) or its relative structural changes, the relative changes of the form factors ($\Delta P(Q)$; Fig. 6a, medium panel, red, gray, and black small open circles, corresponding to the right vertical axis).

**Relative structural changes in the dried immobilized IgM after different treatments**

The dried samples (Fig. 6a) resemble the product as it is used for prolonged storage. The structure signals of the untreated dried, immobilized IgM$_{Fas}$
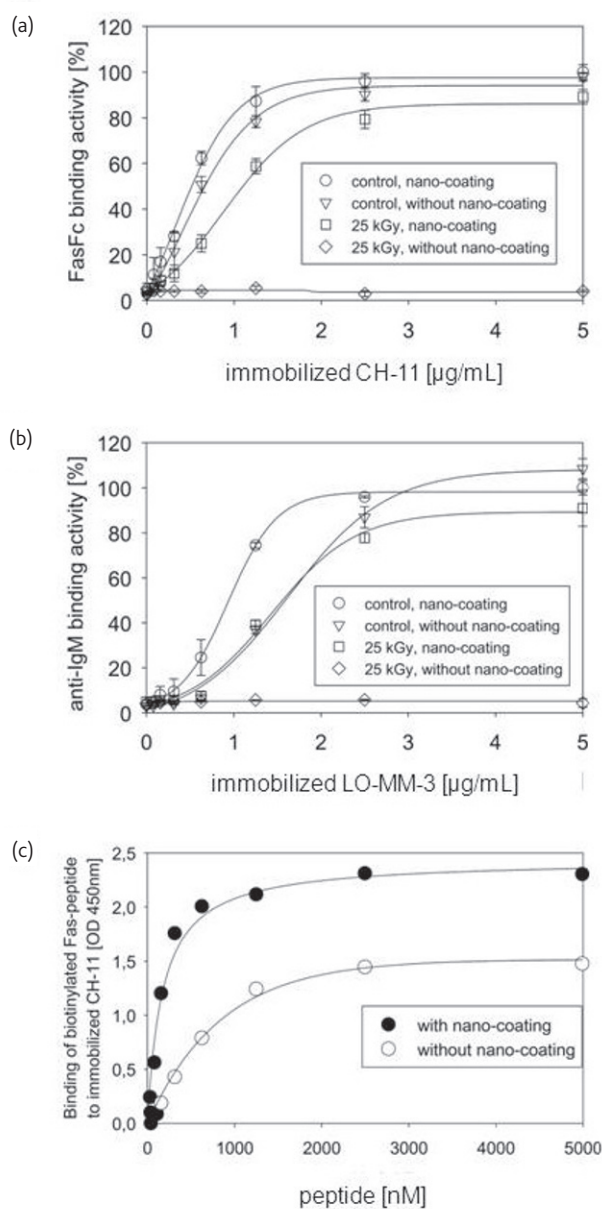


Fig. 7 Preservation of IgM$_{Fas}$ epitope recognition after nano-coating by ELISA. (a,b) Binding of immobilized IgM$_{Fas}$ ((a) CH-11; (b) LO-MM-3) to graded amounts of recombinant human Fas antigen fragment (hFas::Fc) after $\beta$-irradiation and/or nano-coating. (c) Binding of immobilized IgM$_{Fas}$ to graded amounts of epitope peptide after $\beta$-irradiation and/or nano-coating. For $K_D$ determination, data were fitted to a 1:1 Langmuir binding model.

antibody on the PU foam (PU-IgM$_{Fas}$) were at the lower limit of resolution when compared to the background signal of PU alone. Thus it was not possible to calculate the background-corrected scattering-contrast $I(Q)$ and the resulting form factor $P(Q)$ corresponding to the shape of the immobilized untreated IgM$_{Fas}$ molecules in the real space on the PU. Hence, we calculated the relative changes of the calculated form factors for the whole samples (PU in combination with IgM$_{Fas}$), $\Delta P(Q)$ (negative
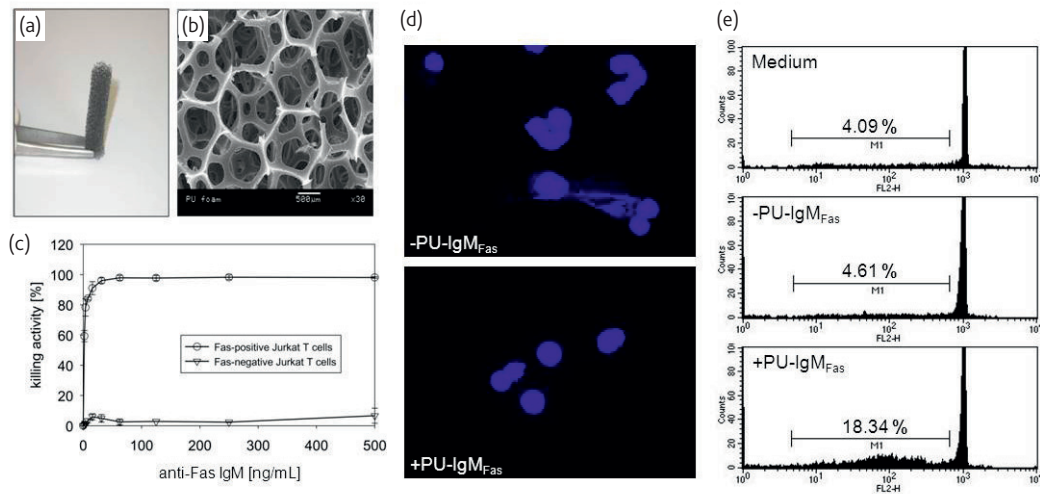
Fig. 8 *Apoptosis induction by PU-IgM$_{Fas}$. Macroscopic (a) and raster electron microscopic (b) photography of PU foam samples. PU foam samples were cut into cylindrical pieces (here: 3 cm³) for the apoptosis induction assays. The pore diameter of open porous PU foam was approximately 1.5 – 2 mm. (c) Effects of PU-IgM$_{Fas}$ containing different concentrations of anti-Fas IgM on the induction of apoptosis in Fas-positive and Fas-negative Jurkat T-cells. (d,e) Ex vivo detection of apoptosis in neutrophils from severely injured patients by fluorescent staining ((d), condensation of nuclei) and by propidium iodide staining and flow cytometry ((e), DNA-strand fragments).*

relative values 1 – 10), of the dried immobilized IgM$_{Fas}$ antibodies, exposed to radiation (*PU-IgM$_{Fas}$), after nano-coating (PU-IgM$_{Fas}$-NC), after nano-coating and subsequently exposed to radiation (*PU-IgM$_{Fa}$s-NC) with respect to the untreated samples (PU-IgM$_{Fas}$). Results are shown in Fig. 6a (medium panel, red, gray, and black small open circles, corresponding to the right vertical axis).

The greatest differences in the form factors were found when untreated PU-IgM$_{Fas}$ samples were compared with PU-IgM$_{Fas}$–NC (Fig. 6a, medium panel, small red open circles). The coating decreased the scattering contrast for characteristic distances between ζ = 3 and ζ = 15 nm on the PU particle. These distances correspond to the average extension of the IgM molecule on the surface of the PU foam and provide evidence that the IgM molecules are entirely coated. Nano-coating and subsequent drying of the immobilized IgM molecule may lead to a conformational change in the dried protein with respect to the untreated dried PU-IgM$_{Fas}$.

When the form factors of the untreated PU-IgM$_{Fas}$ samples were compared with the irradiated *PU-IgM$_{Fas}$ without nano-coating (Fig. 6a, medium panel, small gray open circles), we again observed a significant decrease in scattering contrast due to radiation-mediated conformational changes and possibly bond breakage within the protein leading to a decrease of electronic contrast. When we compared the forms of the untreated PU-IgM$_{Fas}$ with nano-coated and subsequently irradiated *PU-IgM$_{Fas}$–NC (Fig. 6a, medium panel, small black open circles), the relative difference in scattering contrast was lower probably due to radiation-mediated amplification of interactions between NC-excipients and the IgM.

**Protein structure reconstruction of the dried IgM.**
The scattering profiles of the dried samples *PU-IgM$_{Fas}$, PU-IgM$_{Fas}$–NC, and *PU-IgM$_{Fas}$–NC were comparable. Thus, the molecular structures of the IgG subunits, the pentameric IgM molecules and the mean forces

between the IgG arms within the pentameric IgM's were deduced from averaged profiles of dried, differently treated PU-IgM$_{Fas}$ samples. According to the applied analytical model, we fitted the measured background-corrected scattering profiles, leading to the form factor $P(Q)$ of the IgG subunit and the corresponding average size of the IgG arm of k ≈ 4.0 - 6.0 nm (Fig. 6a, dashed lines), related to the radius of gyration ($R_G$). Based on the known three-dimensional structure of the IgG unit cell (Protein Data Bank: 2RCJ)[22], we reconstructed the IgG subunits of the dried immobilized IgM molecules as depicted by the gray bead model in Fig. 6a (upper panel). Further computational operations determined the spatial arrangements of the IgG subunits within the pentameric IgM molecules, particularly κ$_p$, a circular measure that spans two opposite IgG arms and subsequently their opening angles θ. The meaning of the corresponding parameter fractal dimension $D$ is illustrated on the top of Fig. 6, designated "wrinkled structure models". $D$ is related to the particular opening angles θ (Fig. 6, upper panel) that comprise the five IgG arms. All dried systems have a common fractal dimension of $D$ = 3. We anticipated that all dried samples have a common IgM superstructure with q ≈ 0.51° or q ≈ 29.22° for the IgG arms.

The mean forces between the IgG arms are given at the bottom of Fig. 6a (small open connected circles). The high corrugation of the mean forces indicates a closed and collapsed protein structure due to the lack of a hydration shell after drying.

The black lines in Fig. 6a–c; upper panels give the full fit of the SAXS data based on the gray IgG structural models and their mean forces. The anticipated corresponding IgM structures of the dried samples *PU-IgM$_{Fas}$, PU-IgM$_{Fas}$-NC, and *PU-IgM$_{Fas}$-NC are given in Fig. 6a by the green bead model.

**Protein structure reconstruction of the rehydrated IgM.**
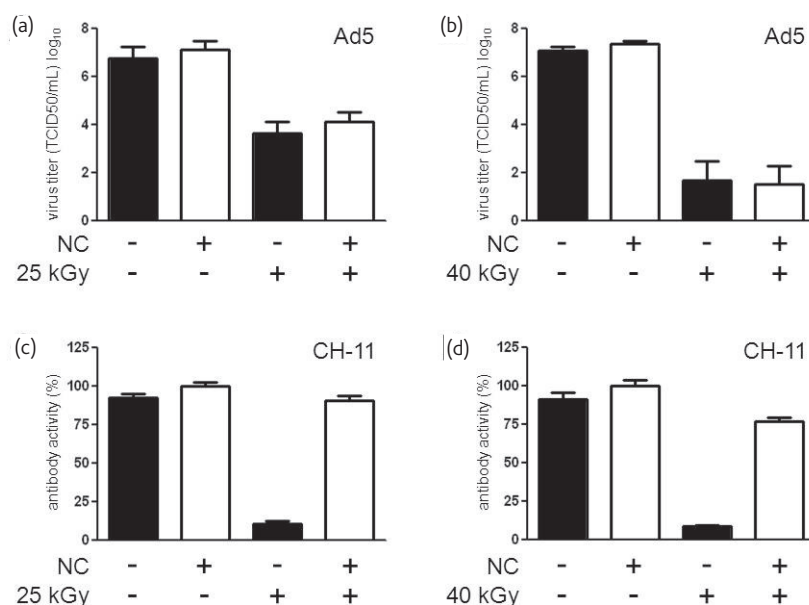After rehydration of the nano-coated and non-coated samples and

Fig. 9 Adenovirus type 5 (Ad5) infectivity assay. (a,b) Ad5 samples were β-irradiated at 25 kGy (a) and 40 kGy (b) with and without nano-coating. The titers of infective virus particles before and after irradiation are shown. (c,d) In the same setting an IgM antibody was irradiated. The relative antigen binding capacity before and after irradiation is shown.

reconstitution of the hydration shell, the scattering contrast for all samples was positive compared with the dried samples. In the case of the rehydrated PU-IgM$_{Fas}$ without nano-coating, the fractal dimension decreased to $D = 2.5$ representing a limited refolding, partially open IgM superstructure, and increased angle θ. The corrugation of the corresponding mean forces is decreased (bottom of Fig. 6b) because the IgG arms are less attracted to each other resulting in a partially open configuration of the IgM superstructure. No measurable signals were obtained for the irradiated and destroyed *PU-IgM$_{Fas}$ without nano-coating.

The opening of the IgM superstructure and thus refolding was even better when the nano-coated PU-IgM$_{Fas}$-NC and the nano-coated and subsequently irradiated *PU-IgM$_{Fas}$–NC samples were rehydrated. The structural model for the IgG arms, representative for both variants is depicted as the gray bead model in Fig. 6c, upper panel. As the fractal dimension decreased to $D = 1.5$, the angle θ increases. When the structural model and the opening angle θ were combined, a rather open structural model for the IgM molecule could be reconstructed (green bead model in Fig. 6c, upper panel). The calculated mean forces showed that the corrugation was lower compared with the other examples given in Fig. 6 (bottom) indicating that nano-coating favors protein rehydration and refolding.

### Functional evaluation of antigen binding by immobilized anti-Fas IgM

To confirm that the immobilized antibody maintains the biological function to specifically recognize and bind the respective antigens even after drying, irradiation, and reconstitution, functional antibody-antigen binding experiments were performed. IgM$_{Fas}$ was immobilized and probed for binding of a highly specific recombinant human Fas antigen fragment (hFas:Fc)[28] with and without nano-coating and/or β-irradiation. As shown in Fig. 7a,b, h$_{Fas}$:Fc was recognized by IgM$_{Fas}$ in a concentration dependent manner. Without protection, β-irradiation at > 25 kGy led to complete loss of antigen binding capacity. By contrast, nano-coating protected IgM$_{Fas}$ from radiation-mediated damage over a broad range of concentrations. In order to investigate the functional integrity of the IgM$_{Fas}$ paratopes at the molecular level, we employed an N-terminally biotinylated epitope peptide (biotin-RCKPNFFCNSTVCEHCDP-NH2) which was identified by peptide array screening. IgM$_{Fas}$ was immobilized on an ELISA plate (with and without β-irradiation and/or nano-coating) and probed with graded amounts of epitope peptide, which was subsequently detected by a streptavidin-HRP conjugate in a colorimetric assay. For reference, the affinity (depicted as equilibrium binding constant (K$_D$)) of IgM$_{Fas}$ for the epitope peptide without coating and β-irradiation was determined to be 160 ± 13 nM (data not shown). As shown in Fig. 7c, β-irradiation led to a drastically reduced affinity of IgM$_{Fas}$ for the epitope peptide (K$_D$ = 855 ± 129 nM), demonstrating severe radiation-induced damage. By contrast, the integrity of the antibody paratopes was fully maintained when nano-coating was applied prior to β-irradiation, demonstrated by preservation of the K$_D$ of the IgM$_{Fas}$ for the epitope peptide (188 ± 25 nM).
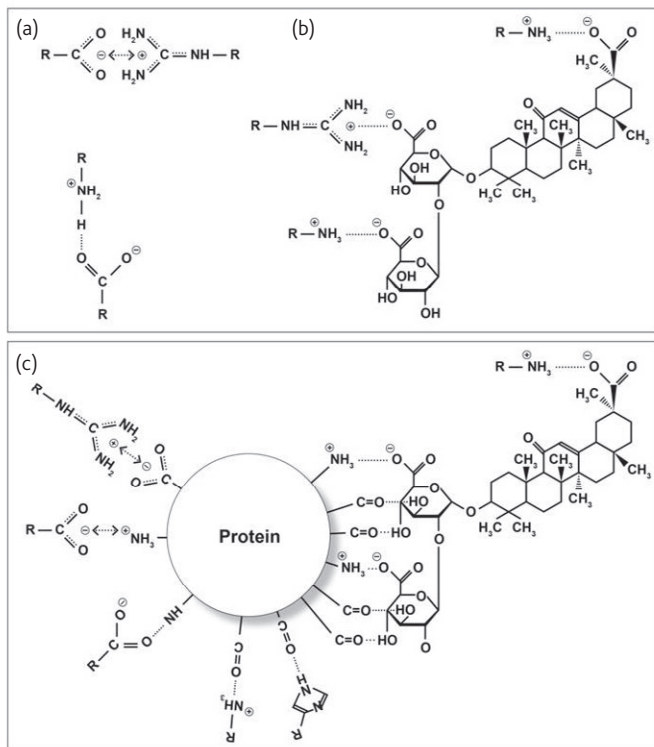
Fig. 10 Proposed mechanism of the nano-coating solution. (a) Interactions between the multiple functional groups of amino acids in solution and particularly during drying. (b) Interactions between basic functional groups of the amino acids with the anionic carboxyl groups within the glycyrrhizic acid molecule, triggering the formation of a highly amorphous state. (c) Sequential substitution of the stabilizing hydrogen bonds between protein and water molecules (hydrate shell) by stabilizing molecular interactions between protein, amino acids, and glycyrrhizic acid in the dried and amorphous states.

### Functional evaluation of the agonistic biological activity of PU-IgMFas-NC

To further confirm the proof of principle that the PU-IgM$_{Fas}$-NC (Fig. 8a/b) not only binds the specific antigen but indeed may agonistically stimulate the Fas receptor on target cells, we studied the potential of PU-IgM$_{Fas}$-NC to induce apoptosis[36-39] and by this to inactivate Fas-sensitive cells *in vitro*[40]. As shown in Fig. 8c, apoptosis induction occurred exclusively in Fas-positive cells after incubation with PU-IgM$_{Fas}$–NC. Moreover, to study the potential therapeutic efficacy of PU-IgM$_{Fas}$–NC in a clinically relevant setting, we used highly activated Fas-expressing neutrophils obtained from trauma patients[38]. Indeed, we confirmed PU-IgM$_{Fas}$-NC-mediated apoptosis in patient neutrophils. Specifically, apoptosis-related condensation of the neutrophil nuclei[40] was found in PU-IgM$_{Fas}$–NC-treated cells but not in untreated cells as demonstrated by nucleic staining (Fig. 8D) and flow cytometry (Fig. 8e) after challenging these neutrophils *ex vivo* with PU-IgM$_{Fas}$–NC for 4 h.

### Sterilization of nano-coated materials

The bioburden[41,42] of functionalized and nano-coated polyurethane foams was determined. The bioburden (number of infectious contaminating particles) is an important parameter for the sterility of a medical device and of high relevance for the approval of such devices. Six different lots of each >70 plastic housings containing PU-IgM$_{Fas}$–NC were manufactured for potential use for extracorporeal immune modulation. The bioburden of 10 non-sterile PU-IgM$_{Fas}$–NC samples from each lot was measured for reference. The mean bioburden was 151 ± 18 bacteria/fungi per module. Sterilization was performed by β-irradiation at ≥ 25 kGy, and validation of sterilization was performed according to the ISO 11137 VD$_{max}$ method[41,42]. All 60 PU-IgM$_{Fas}$–NC modules irradiated with the reference dose (8.5 ± 0.8 kGy) were found to be sterile.

Virus inactivation studies were performed using human adenovirus type 5 (Ad5) as a reference virus[25-27]. After β-irradiation, the virus/protective solution bilayer was resuspended and the TCID$_{50/ml}$ was determined by end-point titration (Fig. 9a,b). In parallel, the same experimental setup was employed with IgM (LO-MM-3; Fig. 9c,d). β-irradiation led to quantitative inactivation of Ad5 (25 kGy, ≥ 99.9 % reduction, 40 kGy ≥ 99.999 % reduction; Fig. 9a,b) while the antibody functionality was maintained.

## Discussion

The major challenge in the development of bio-functionalized medical devices and functionalized nano-particles[43-45] is the limited stability of immobilized proteins during production and storage and, most importantly, the loss of biological function during sterilization.

We showed the efficacy of a novel protein stabilization technology (nano-coating) during irradiation of biocompatible carriers. As an example, immunomodulatory IgM antibodies covalently coupled to open porous PU foam for extracorporeal immune therapy were used. Our results prove that the nano-coating technology enables the development of end-sterilized bio-functionalized materials without loss of biological function and safety.

The physico-chemical characteristics of the nano-coating technology were shown to fulfill the requirements for effective three-dimensional stabilization of proteins during drying, sterilization, and reconstitution. To confirm this, we studied the morphological modifications of a large and irradiation-sensitive anti-Fas IgM antibody coupled to medical-grade polyurethane by SAXS analysis. SAXS allows for monitoring of structural changes of the protein coupled to a solid carrier upon physical stress. The principle of the SAXS method[23,24] has been described in detail earlier and the underlying algorithms were specifically adapted to analyze the nano-molecular integrity of IgM antibodies coupled to biocompatible carrier materials. We were able to prove that (i) covalently immobilized IgM molecules are present on PU after drying, sterilization, and reconstitution, (ii) the protein is embedded in a nano-coating shell after drying, and (iii) the three-dimensional protein structure is stabilized, and refolding after reconstitution is improved by nano-coating.

The agonistic anti-Fas containing open porous PU foam (PU-IgM$_{Fas}$) has been developed for use in extracorporeal immune modulation devices. The therapeutic concept is to treat patients with severe immune disorders such as systemic inflammatory response syndrome (SIRS) or sepsis by rapid inactivation of hyper-activated neutrophils within the blood circulation[19,36,37] via extracorporeal inactivation of these cells by agonistic Fas signaling[19,38].

By means of functional *in vitro* and *ex vivo* read-out assays, we

confirmed the efficacy and clinical relevance of nano-coating by showing the preservation of specific antigen/epitope binding of $IgM_{Fas}$ during irradiation. Moreover, when hyper-activated neutrophils from severely injured patients at risk for developing SIRS were challenged *ex vivo* with $PU-IgM_{Fas}$, neutrophil apoptosis was induced by $PU-IgM_{Fas}$.

The validity of standard sterilization of $PU-IgM_{Fas}$ was demonstrated in accordance with the ISO 11137 $VD_{max}$[41,42] method resulting in a Sterility Assurance Level of $10^{-6}$. Additionally, our virus contamination experiments revealed a sufficient irradiation-mediated reduction of infectious virus particles, even in the presence of nano-coating whereas functionality of $IgM_{Fas}$ was preserved.

In Fig. 10, the hypothesized interactions between amino acids (Fig. 10a), amino acids with glycyrrhizic acid (Fig. 10b), and amino acids/glycyrrhizic acid with protein structures (Fig. 10c), are depicted schematically. In this model, glycyrrhizic acid interacts with both the protein (via ionic interactions and hydrogen bonds) and small molecules (e.g., amino acids via three carboxyl groups of the glycosidic part and the aglycon). According to the preferential exclusion concept, glycyrrhizic acid together with uncharged molecules may support the osmolytic stabilization of the hydration shell around the immobilized protein in the presence of water by increasing the surface tension of the aqueous solutions. Interactions between different amino acids, as well as between amino acids and glycyrrhizic acid, result in the strong amorphous character of the nano-coating solution. Moreover, during drying, the protein is interconnected with glycyrrhizic acid and with charged amino acids that replace the water molecules while interacting with the protein via hydrogen bonds according to the concept of preferential binding (Fig. 10c). The amorphous character in combination with the antioxidant, radical scavenging, and metal chelating features of particular components supports the protective effects of nano-coating.

In conclusion, the presented NC procedure will facilitate the application of biologic-device combination products since it enables inexpensive terminal sterilization of a broad range of bio-functionalized materials (Table 1) while preserving optimal conditioning of the bioactive surface. mt

### Instrument citation

X-ray diffractometer XRD 3000 TT (Seifert, Germany)
X-ray reflectometer Bruker D8 (Bruker AXS, Germany)
Profilometer Veeco, Dektak 3030 (Capovani Brothers Inc., US)
Mettler Toledo 821e (Giessen, Germany)
Falling Ball Viscometer model AMVn, Anton Paar (Ostfildern, Germany)
Rotating anode generator (Nanostar, BRUKER AXS)
MultiPep RS instrument (Intavis, Köln, Germany)

### References

1. Han, Q., *et al., Biomaterials* (2010) **31**(35), 9212.
2. Hosper, N. A., *et al., Biomaterials* (2010) **31**(14), 3910.
3. Sawyer, A. A., *et al., Biomaterials* (2009) **30**(13), 2479.
4. Drake, M. P., *et al., J Am Chem Soc* (1957) **79**, 1395.
5. Gianfreda, L., and Scarfi, M. R., *Mol Cell Biochem* (1991) **100**(2), 97.
6. Kapoor, S., and Priyadarsini, K. I., *Biophys Chem* (2001) **92**(1-2), 119.
7. Stadtman, E. R., and Levine, R. L., *Ann N Y Acad Sci* (2000) **899**, 191.
8. Zbikowska, H. M., *et al., Free Radic Biol Med* (2006) **40**(3), 536.
9. Garrison, W. M., *et al., Radiat Res* (1962) **16**, 483.
10. Arakawa, T., *et al., Adv Drug Deliver Rev* (2001) **46**(1-3), 307.
11. Han, Y., *et al., Arch Pharm Res* (2007) **30**(9), 1124.
12. Jain, N. K., and Roy, I., *Protein Sci* (2009) **18**(1), 24.
13. Jorgensen, L., *et al., Expert Opin Drug Del* (2009) **6**(11), 1219.
14. Arakawa, T., *et al., Amino Acids* (2007) **33**(4), 587.
15. Auton, M., *et al., Proteins* (2008) **73**(4), 802.
16. Shimizu, S., and Smith, D. J., *J Chem Phys* (2004) **121**(2), 1148.
17. Timasheff, S. N., *Annu Rev Bioph Biom* (1993) **22**, 67.
18. Timasheff, S. N., *P Natl Acad Sci USAa* (2002) **99**(15), 9721.
19. Scholz, M., and Cinatl, J., *Med Res Rev* (2005) **25**(3), 331.
20. Fadeel, B., *et al., Int Immunol* (1998) **10**(2), 131.
21. Peter, M. E., *et al., Cell* (2007) **129**(3), 447.
22. Perkins, S. J., *et al., J Mol Biol* (1991) **221**(4), 1345.
23. Horejs, C., *et al., ACS Nano* (2011) **5**(3), 2288.
24. Horejs, C., *et al., J Chem Phys* (2010) **133**(17), 2288.
25. DVV, *(German Association for the Control of Virus Diseases) and Robert Koch Institute (RKI; German Federal Health Authority); Hygiene & Medizin* (2009) **34**, 293.
26. Kim, I. S., *et al., J Microbiol Biotechn* (2008) **18**(5), 997.
27. Sauerbrei, A., *et al., J Hosp Infect* (2007) **65**(3), 264.
28. Schneider, P., *et al., J Biol Chem* (1997) **272**(30), 18827.
29. Nicoletti, I., *et al., J Immunol Methods* (1991) **139**(2), 271.
30. Brandt, O., *et al., Curr Chem Biol* (2009) **3**, 171.
31. Dietrich, U., *et al., Curr Pharm Biotechnol* (2012), in press.
32. Koch, J., *Mini Rev Organ chem* (2011) **8**, 111.
33. Koch, J., and Mahler, M., *Peptide Arrays on Membrane Supports: Synthesis and Applications*, Springer, Heidelberg (2002).
34. Plewnia, G., *et al., J Mol Biol* (2007) **369**(1), 95.
35. Hilpert, K., *et al., Nature Protocols* (2007) **2**(6), 1333.
36. Logters, T. T., *et al., J Inflamm* (London, England) (2010) **7**, 18.
37. Paunel-Gorgulu, A., *et al., Immunobiology* (2011) **216**(3), 334.
38. Paunel-Gorgulu, A., *et al., J Immunol* (2009) **183**(10), 6198.
39. Scholz, M., *et al., Asaio* J (2005) **51**(2), 144.
40. Zamzami, N., and Kroemer, G., *Nature* (1999) **401**(6749), 127.
41. ISO1137-1:2006.
42. ISO1137-2:2006.
43. Cedervall, T., *et al., P Natl Acad Sci USA* (2007) **104**(7), 2050.
44. Monopoli, M. P., *et al., J Am Chem Soc* (2011) 133 (8), 2525.
45. Walczyk, D., *et al., J Am Chem Soc* (2010) **132** (16), 5761.